

Nature of the activity-mediated unjamming transition in confluent cell monolayers

Souvik Sadhukhan,^{1,*} Chandan Dasgupta,^{2,3,†} and Saroj Kumar Nandi^{1,‡}

¹Tata Institute of Fundamental Research, 36/P Gopanpally Village, Hyderabad - 500046, India

²Department of Physics, Indian Institute of Science, Bangalore 560012, India

³International Centre for Theoretical Sciences, TIFR, Bangalore 560089, India

Activity-mediated unjamming transition in confluent systems is crucial for embryogenesis, wound healing, cancer metastasis, etc. During these processes, the cells progressively change their junction properties, characterized by an interaction parameter p_0 , and become motile. How does activity affect this unjamming transition? Using molecular dynamics simulations of the active Vertex model and analytical mode-coupling theory (MCT), we show that the nature of the transition in the presence of activity remains similar to that in equilibrium. The agreement of the simulation results with the MCT predictions demonstrates that the structure-dynamics feedback mechanism controls the relaxation dynamics. In addition, we present the first computation of a dynamic length scale, ξ_d , and show that the growing relaxation time accompanies an increasing ξ_d . Furthermore, unlike particulate glasses, the static length is proportional to ξ_d . Our results highlight the unique nature of the glassy dynamics in confluent systems and rationalize the existing experimental data.

I. INTRODUCTION

Metastasis is the leading cause of death in cancer patients [1, 2]. It has several steps, where the cancer cells leave their primary sites, go through the stroma and other tissues, use the bloodstream, and acclimatize at a secondary site [1, 3–5]. The primary step of this process is cellular unjamming [6, 7]. Many past works have shown that an epithelial monolayer shows glassy behavior where the system has anomalously slow dynamics with a stretched exponential relaxation [8, 9], non-Gaussian displacement distribution [9–11], spatially heterogeneous dynamics [8, 12], etc. During several biological processes, such as embryogenesis [13–15], wound-healing [16–19], and cancer progression and metastasis [7, 20–24], the cells undergo an epithelial-to-mesenchymal transition (EMT) [25–28]. The epithelial monolayer is primarily sedentary, where cells show strong cell-cell adhesion and out-of-plane polarity. By contrast, the cancerous monolayer is dynamic, where cells show weak cell-cell adhesion, develop in-plane polarity, and become motile [7, 25, 29]. Although EMT was thought of as a binary switch between the epithelial and mesenchymal states, it is now clear that it is more like a continuum than a switch [28, 30–32]. At the early stage of EMT, known as partial EMT or pEMT, the monolayer remains confluent, although the cells become motile. Cellular motility facilitates unjamming [7, 33]; a more detailed characterization of the transition is essential for a deeper understanding of metastasis.

Experiments have shown contrasting results for different oncogenes. For example, human breast cancer cells MCF-10A fluidizes by the over-expression of an oncogene, 14 – 3 – 3 ζ , or an endocytic protein, RAB5A [23]. However, the same monolayer solidifies by over-expressing another oncogene ErbB2/HER-2/neu [10]. A recent work has shown that confluency has a nontrivial effect on activity, where the former leads to an effective rotational diffusivity, D_r^{eff} , that is different from the intrinsic rotational diffusivity, D_r , of motility

[34]. Thus, how activity will affect the glassy dynamics is nontrivial. Furthermore, simulations suggest that within the continuum of pEMT [34, 35], during the initial times when cellular junctions are relatively strong, the monolayer shows super-Arrhenius relaxation. Conversely, at a later time, when junctions become weaker, the monolayer shows sub-Arrhenius relaxation. In this work, we focus on this later regime. Using large-scale molecular dynamics simulations of the active Vertex model and an analytical theory, the mode-coupling theory (MCT) of glasses [36–38], we investigate the effects of motility on the unjamming transition. What is the specific nature of this transition? How does the dynamics of a monolayer with pEMT differ from that of the epithelial states? Does the structure-dynamics correlation of confluent epithelial systems [39–41] survive even under motility?

We have simulated the athermal active vertex model with the energy function \mathcal{H} (see supplementary material (SM), Sec. S1 for details),

$$\mathcal{H} = \sum_{i=1}^N [\lambda_A (a_i - a_0)^2 + \lambda_P (p_i - p_0)^2], \quad (1)$$

where N is the total number of cells; a_i and p_i are the area and perimeter of the i th cell; a_0 and p_0 are the target area and target perimeter; λ_A and λ_P are two elastic constants [9, 42–44]. p_0 parameterizes the intercellular interaction and is a control parameter of dynamics. We have taken a 50 : 50 binary mixture with $a_{0\alpha} = 0.8$ and $a_{0\beta} = 1.2$ to avoid crystallization, and designate the system via $p_0 = p_{0\alpha}/\sqrt{a_{0\alpha}} = p_{0\beta}/\sqrt{a_{0\beta}}$. We simulate the system via molecular dynamics in the overdamped regime with friction $\mu = 1$ (see SM). We implement activity by assigning each vertex k with a self-propulsion force $\mathbf{f}_a^k = f_0 \hat{\mathbf{n}}_k$, where $\hat{\mathbf{n}}_k = (\cos \phi_k, \sin \phi_k)$ gives the direction and f_0 is the strength. The angle, ϕ_k , performs a random walk with persistence time $\tau_p = 1/D_r$. We use $\sqrt{a_0}$ as the unit of length, where a_0 is the average area, and $1/\lambda_A \mu a_0$ is the unit of time.

To take advantage of the effective equilibrium scenario at small τ_p , we fix $D_r = 1/\tau_p = 1$ and study the properties with varying f_0 [45–47]. Since we set $\mu = 1$, f_0 is numeri-

* ssadhukhan@tiffr.res.in

† cdgupta@iisc.ac.in

‡ saroj@tiffr.res.in

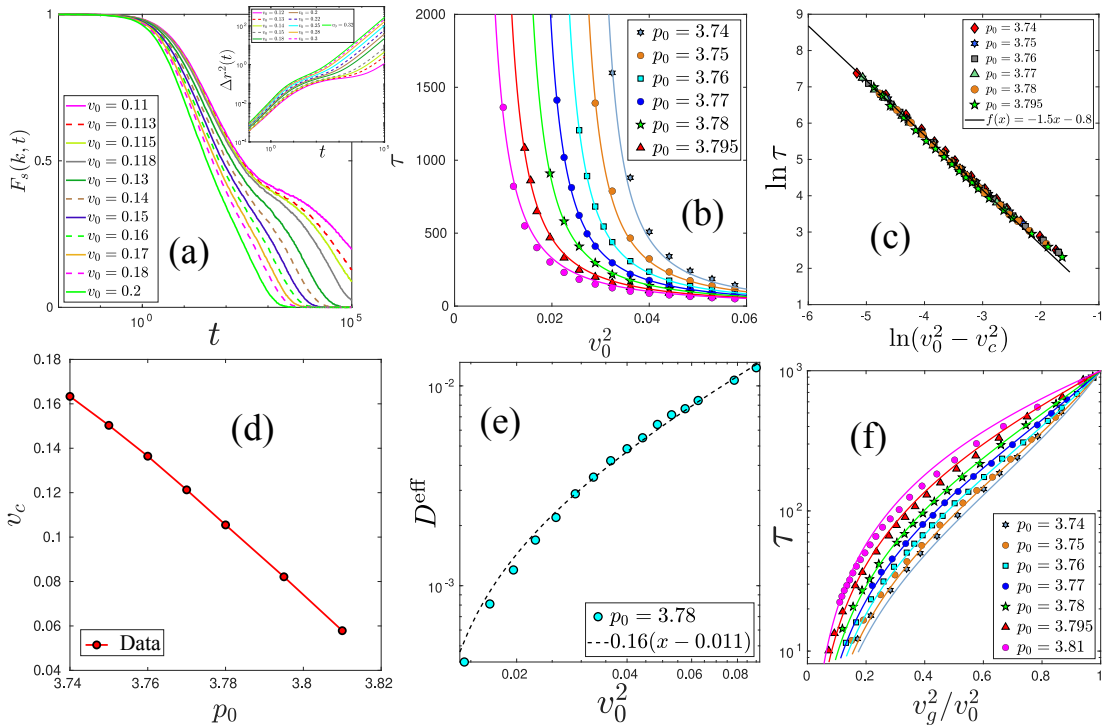


FIG. 1. Comparison of simulation data on AVM with MCT: (a) Evolution of the self intermediate scattering function, $F_s(k, t)$ for various v_0 and $p_0 = 3.78$. **Inset:** Mean-square displacement for the corresponding parameters as in the main figure. (b) The relaxation time, τ , as a function of v_0^2 for different p_0 . The points are simulation data, and the lines denote fits with Eq. (4). (c) Plot of $\log(\tau)$ as a function of $\log(v_0^2 - v_c^2)$ for various p_0 shows a data collapse to a master curve as $\gamma = 3/2$ and A are constants. The line represents a linear fit with the slope $3/2$. (d) The MCT transition point, v_c , monotonically decreases with p_0 . (e) The effective diffusion constant, D^{eff} , goes to zero as a power-law as v_0 tends to v_c , but with a different exponent than γ , signifying the breakdown of the Stokes-Einstein relation. (f) Angell plot representation of τ : $\log(\tau)$ is plotted against v_g^2/v_0^2 . v_g is defined as the value of v_0 when τ reaches 10^3 . It shows a sub-Arrhenius relaxation. Data presented here are for $D_r = 1$ and $N = 256$.

cally the same as the self-propulsion velocity, v_0 . We present the results in terms of v_0 using v_0^2 in place of temperature T to characterize the transition. Reference [41] has shown that MCT works surprisingly well for epithelial systems. Here, we take a similar approach. We test the applicability of the MCT by comparing the relaxation dynamics with the MCT predictions. We show that MCT remains valid even in the presence of activity; thus, the structure-dynamics correlation holds, and the feedback mechanism of MCT controls the dynamics. The relaxation time, τ , diverges with the same exponent, $\gamma = 3/2$, as in equilibrium [41]; this indicates that the relaxation dynamics remains equilibrium-like, much like that in particulate active systems at small τ_p [9, 46–49]. In addition, we present the first computations of the dynamic length scale, ξ_d , in confluent systems. ξ_d also diverges at the critical point, and the increasing τ accompanies a growing ξ_d .

II. RESULTS

We characterize the dynamics via the self-intermediate scattering function, $F_s(k, t)$, defined as

$$F_s(k, t) = \langle \tilde{F}_s(k, t) \rangle = \frac{1}{N_\alpha} \left\langle \sum_{i=1}^{N_\alpha} \exp[i\mathbf{k} \cdot (\mathbf{r}_i(0) - \mathbf{r}_i(t))] \right\rangle \quad (2)$$

where, k is the magnitude of the wave-vector \mathbf{k} , N_α , the number of cells with target area $a_{0\alpha}$, \mathbf{r}_i , the centre of mass of the i^{th} cell. The angular brackets denote the ensemble and time averaging. We consider only the α -particles for the calculation of $F_s(k, t)$ [50, 51]. We present the results for the k corresponding to the first peak of the structure factor. Figure 1(a) shows the decay of $F_s(k, t)$ for various values of v_0 . The inset of Fig. 1(a) shows the mean square displacement, $\Delta r^2(t)$, defined as

$$\Delta r^2(t) = \left\langle \frac{1}{N} \sum_{i=1}^N (\mathbf{r}_i(t) - \mathbf{r}_i(0))^2 \right\rangle. \quad (3)$$

The characteristic two-step decay of $F_s(k, t)$ is evident at lower values of v_0 . Similarly, $\Delta r^2(t)$ also shows a sub-diffusive behavior at intermediate times and becomes diffusive at long

times (inset of Fig. 1a).

We define the relaxation time, τ , as $F_s(k, \tau) = 0.3$. MCT predicts a power law divergence of τ in thermal systems as the temperature T tends towards a critical value. Translating this result for active systems at small τ_p , we obtain

$$\tau = A(v_0^2 - v_c^2)^{-\gamma}, \quad (4)$$

where v_c is the MCT critical point, A is a constant, and γ is a universal exponent. We obtain τ in our simulation with varying v_0 for several values of p_0 . For a particular p_0 , we fit the data of τ as a function of v_0 with Eq. (4) and obtain A , γ , and v_c . We show these fits for several values of p_0 in Fig. 1(b). We find that $A = 0.71$ and $\gamma = 3/2$ remain constant for various p_0 in the regime of our interest here. Figure 1(c) shows the plot of $\ln \tau$ as a function $\ln(v_0^2 - v_c^2)$: Eq. (4) shows that this should be a straight line with slope $-3/2$ (solid line). The simulation data agree remarkably well with the MCT prediction, Eq. (4). Much like any critical theory, the critical point depends on the system parameters. In the context of the vertex model, p_0 parametrizes the interaction potential; therefore, we expect v_c to vary with changing p_0 . Figure 1(d) shows that v_c monotonically decreases as p_0 increases. We emphasize that although v_c changes with p_0 , the exponent γ in Eq. (4) remains constant; this is consistent with the universal prediction of the theory. In addition, MCT predicts power-law decay of $F_s(k, t)$ around the plateau (β -regime), and the simulation results are consistent with these predictions (see SM, Sec. S2).

We have also computed the effective diffusion constant, D^{eff} , as the ratio of self-diffusivity and free diffusion constant of an isolated cell. $D^{\text{eff}} = D_s/D_0$ where $D_s = \lim_{t \rightarrow \infty} \langle \Delta r^2(t) \rangle / (4t)$ and $D_0 = v_0^2 / 2D_r$. $D^{\text{eff}} \rightarrow 0$ when τ diverges. Fitting the data of D^{eff} with the power law form of MCT, $D^{\text{eff}} = A'(v_0^2 - v_c^2)^{\gamma'}$, we obtain the same v_c as from the data of τ , and $\gamma' = 1$. We show the fit of D^{eff} for $p_0 = 3.78$ in Fig. 1(e). Note that the exponent γ in Eq. (4) and γ' are different, implying the violation of the Stokes-Einstein relation (SER) [51–53]. This breakdown is similar to what one finds in particulate systems, where MCT predicts that SER remains valid, but simulations show a violation [54] (see however Ref. [55]). We will explore this breakdown of SER in detail in a separate work. Finally, we show the Angell plot representation of τ as a function of v_g^2/v_0^2 , where we have defined $\tau(v_g) = 10^3$ in Fig. 1(f). Consistent with the agreement of simulation results with MCT, the relaxation dynamics shows a sub-Arrhenius behavior [41].

Next, we calculate the four-point susceptibility, $\chi_4(k, t)$, defined as the fluctuations in $F_s(k, t)$, as follows,

$$\chi_4(k, t) = N_\alpha [\langle \tilde{F}_s(k, t)^2 \rangle - \langle \tilde{F}_s(k, t) \rangle^2], \quad (5)$$

where $\tilde{F}_s(k, t)$ is defined in Eq. (2). $\chi_4(k, t)$ gives the measure of dynamic heterogeneity (DH) in glassy systems. As t increases, $\chi_4(k, t)$ grows from zero, reaches a maximum, and then decays to zero at long times. We show the behavior of $\chi_4(k, t)$ for k corresponding to the structure factor maximum and $p_0 = 3.78$ for various v_0 in Fig. 2(a). As v_0 decreases,

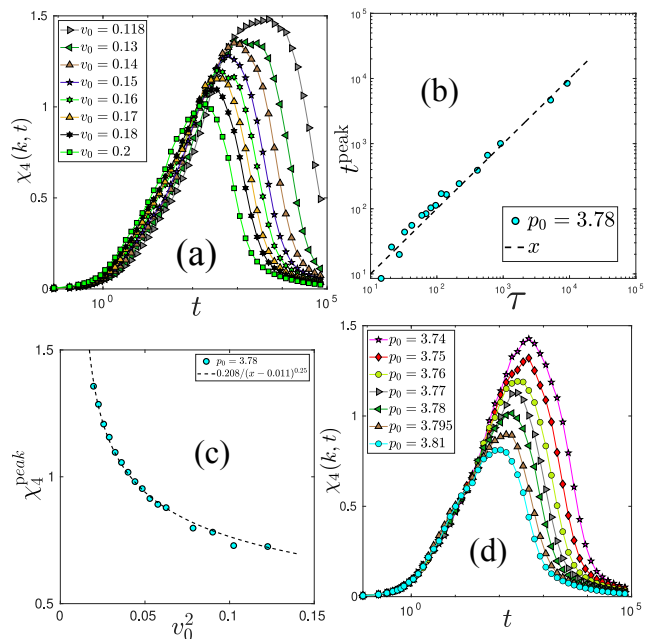


FIG. 2. The behavior of the four-point correlation function, $\chi_4(k, t)$. (a) $\chi_4(k, t)$ has a non-monotonic dependence on t . It grows at short times, reaches a peak, χ_4^{peak} , at time t_{peak} , and then decays towards zero. (b) t_{peak} gives another measure of the relaxation time and is proportional to τ . The dashed line is a linear fit of the data (symbols). (c) χ_4^{peak} diverges as a power law at v_c with the exponent $1/4$. (d) Evolution of $\chi_4(k, t)$ at $v_0 = 0.2$ with varying p_0 . Both χ_4^{peak} and t_{peak} increase as p_0 decreases.

the peak height of $\chi_4(k, t)$, χ_4^{peak} increases. The time, t_{peak} , at which $\chi_4(k, t)$ reaches its maximum, gives another measure of the relaxation time. Typically, one finds $t_{\text{peak}} \propto \tau$ [9, 56]; Fig. 2(b) shows that this relation holds for the active Vertex model. Furthermore, χ_4^{peak} gives a measure of the correlation volume. Figure 2(a) shows that χ_4^{peak} increases as v_0 decreases. We compare χ_4^{peak} with the power-law prediction of MCT: $\chi_4^{\text{peak}} \sim (v_0^2 - v_c^2)^{-\delta}$. The simulation data shows that χ_4^{peak} also diverges at the same v_c with $\delta = 1/4$. We show the fit for $p_0 = 3.78$ in Fig. 2(c); the behavior for other values of p_0 remains similar.

How does $\chi_4(k, t)$ behave at constant activity but varying p_0 ? Figure 2(d) shows $\chi_4(k, t)$ at constant $v_0 = 0.2$ and different values of p_0 . Park *et al.* showed that the monolayers of both asthmatic and non-asthmatic human bronchial epithelial cells become more sluggish as they mature with passing days [8]. As the monolayer matures, the cell-cell junctions become more firm, leading to a decrease in p_0 . In the experiments, it results in decreasing values of the observed perimeter or the shape index [8]. Figure 2(d) shows that as p_0 decreases, t_{peak} and χ_4^{peak} increase. These results rationalize the experimental findings: As the system matures and the junctions become stronger, the system becomes more sluggish, and the volume of dynamically heterogeneous regions increases. We can also

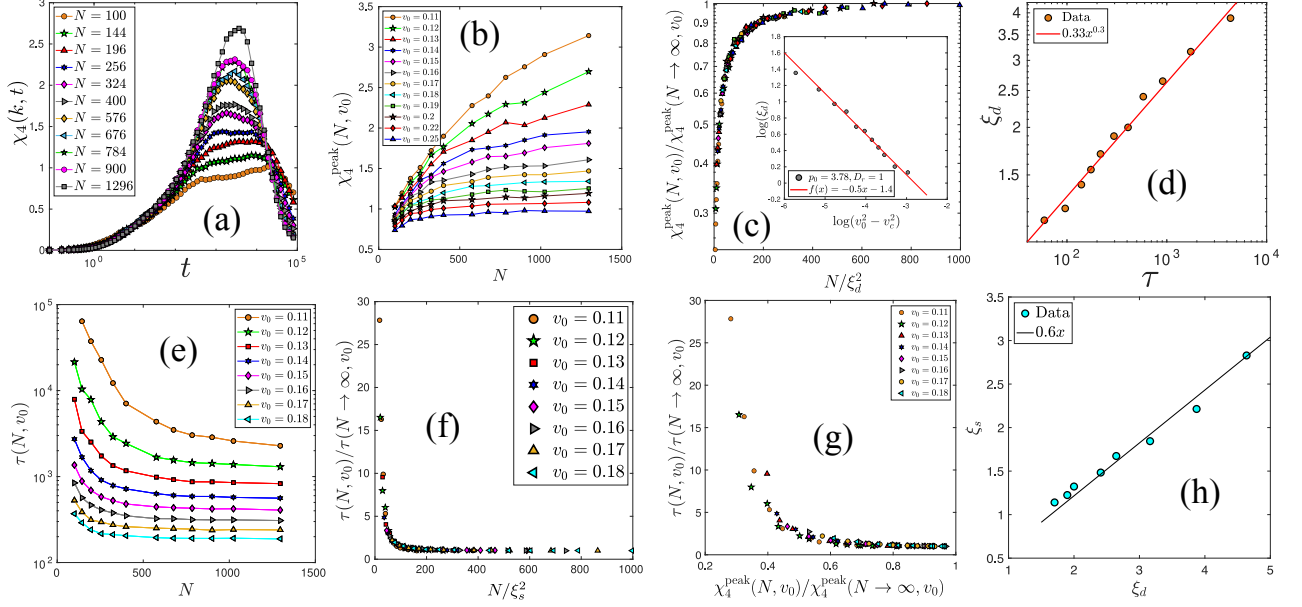


FIG. 3. Finite-size scaling analysis of χ_4^{peak} and τ . (a) $\chi_4(k, t)$ as a function of t for different values of N for $v_0 = 0.12$ and $p_0 = 3.78$. χ_4^{peak} increases and the peak becomes sharper as N increases. (b) $\chi_4^{\text{peak}}(N, v_0)$ as a function N for various v_0 . χ_4^{peak} initially increases with N and then saturates to a v_0 -dependent value. (c) Scaling collapse of $\chi_4^{\text{peak}}(N, v_0)/\chi_4^{\text{peak}}(N \rightarrow \infty, v_0)$ as a function of $N/\xi_d^2(v_0)$. The data collapse for the specific values of $\xi_d(v_0)$ gives the dynamic length scale. **Inset:** Plot of $\log(\xi_d)$ as a function of $\log(v_0^2 - v_c^2)$ shows a linear trend, signifying a power-law behavior. We find the exponent $\nu = 1/2$ from a linear fit (line) of the data (symbols). (d) MCT predicts a power-law relation between ξ_d and τ : $\xi_d \propto \tau^{1/z}$ with $z = \gamma/\nu = 3$. The simulation data (symbols) are consistent with this behavior (line). (e) τ as a function of N for different v_0 , showing that τ initially decreases with N and then saturates to a v_0 -dependent value for large N . (f) Scaling collapse of $\tau(N, v_0)/\tau(N \rightarrow \infty, v_0)$ as a function of $N/\xi_s^2(v_0)$ for appropriate choice of the length scales $\xi_s(v_0)$. (g) Plot of $\tau(N, v_0)/\tau(N \rightarrow \infty, v_0)$ versus $\chi_4^{\text{peak}}(N, v_0)/\chi_4^{\text{peak}}(N \rightarrow \infty, v_0)$ show data collapse for different v_0 and N . (h) Plot of $\xi_s(v_0)$ versus $\xi_d(v_0)$ show that they are proportional to each other.

obtain the DH length scale, ξ_d , from the data of χ_4^{peak} via a finite size scaling, as we demonstrate below.

Within MCT, the glassy dynamics comes from a genuine phase transition where τ diverges concomitantly with the divergence of ξ_d . We first compute $\chi_4(k, t)$, Eq. (5), for several system sizes with N spanning from $N = 100 - 1296$, for different values of v_0 and $p_0 = 3.78$. We show $\chi_4(k, t)$ for $v_0 = 0.12$ for different values of N in Fig. (3a); χ_4^{peak} grows as N increases. Figure 3(b) shows $\chi_4^{\text{peak}}(N, v_0)$, the peak value of $\chi_4(k, t)$ for specific values of N and v_0 , as a function of N for different values of v_0 . $\chi_4^{\text{peak}}(N, v_0)$ initially grows with increasing N and saturates to a v_0 -dependent value as $N \rightarrow \infty$. This behavior indicates the presence of a length scale, ξ_d ; $\chi_4^{\text{peak}}(N, v_0)$ continues to grow with increasing N when ξ_d is larger than the system size and then saturates in the other limit.

According to the finite-size scaling hypothesis, $\chi_4^{\text{peak}}(N, v_0)/\chi_4^{\text{peak}}(N \rightarrow \infty, v_0)$ should be a function of $N/\xi_d^2(v_0)$. To extract the correlation length, we find the values of $\xi_d(v_0)$ for which plots of $\chi_4^{\text{peak}}(N, v_0)/\chi_4^{\text{peak}}(N \rightarrow \infty, v_0)$ as a function of $N/\xi_d^2(v_0)$ for all N and v_0 collapse onto a master curve. Note that in this method, the correlation length $\xi_d(v_0)$ is determined modulo a multiplicative constant: if data collapse is obtained for a set of $\xi_d(v_0)$, a similar data

collapse would be obtained for $c\xi_d(v_0)$ where c is a constant. The data collapse for $p_0 = 3.78$ is shown in Fig. 3(c), and the corresponding values of $\xi_d(v_0)$ are shown in the inset of Fig. 3(c). Following the scaling prediction of inhomogeneous mode-coupling theory (IMCT) for glassy systems [57] and using the effective equilibrium nature of our system, we obtain for our active Vertex model, $\xi_d(v_0) \sim (v_0^2 - v_c^2)^{-\nu}$. We have fitted ξ_d as a function of v_0^2 with this power-law form and obtained the same v_c as before, and $\nu = 1/2$. The inset of Figure 3(c) shows the plot of $\log(\xi_d)$ as a function of $\log(v_0^2 - v_c^2)$ that follows a straight with the slope $\nu = 1/2$. The scaling predictions of ordinary critical phenomenon suggest $\delta = \nu(2 - \eta)$ [58]. Using the values of δ and ν , we obtain $2 - \eta = 1/2$. This value is quite different from the prediction of IMCT [57] and simulation results for passive particulate systems [59, 60]. However, the value is reasonable for a two-dimensional system where the two-point spatial order-parameter correlation function decays as $1/r^\eta$, where r is the spatial distance. MCT is a critical theory that advocates a diverging correlation length, ξ_d , accompanying the divergence of τ . Using the scaling relations for the individual variables, we obtain $\xi_d \sim \tau^{1/z}$ where $z = \gamma/\nu = 3$. We show the behavior of ξ_d as a function of τ in Fig. 3(d) and find the exponent $z \approx 3$.

We have also checked the system-size scaling of the relax-

ation time, τ , for the active confluent cell monolayer. It was found earlier [59] that the system-size dependence of the relaxation time in passive particulate systems is governed by a different correlation length called the static correlation length ξ_s . To check whether a similar result is obtained for the present model, we have plotted τ vs. N for various v_0 as shown in Fig. (3e). As N increases, τ decreases and eventually saturates to a v_0 -dependent value. The saturation value increases with decreasing v_0 . The system-size dependence of τ is similar to that in passive particulate systems [59]. However, it contrasts with the usual dynamical finite-size scaling close to criticality in which the relaxation time increases with system size. We find that $\tau(N, v_0)$ also exhibits a scaling collapse when we plot $\tau(N, v_0)/\tau(N \rightarrow \infty, v_0)$ as a function of $N/\xi_s^2(v_0)$, Fig. (3f), for appropriate choice of $\{\xi_s(v_0)\}$. As shown in Fig. (3g), ξ_s turns out to be proportional to ξ_d , establishing that the system-size dependences of χ_4^{peak} and τ are governed by the *same* correlation length (modulo a multiplicative constant). This is analogous to finite-size scaling in usual critical phenomena but markedly different from the behavior observed in passive glassy systems of particles [59]. As a further check, we have plotted $\chi_4^{\text{peak}}(N, v_0)/\chi_4^{\text{peak}}(N \rightarrow \infty, v_0)$ vs. $\tau(N, v_0)/\tau(N \rightarrow \infty, v_0)$ in Fig. (3h). The data points for different v_0 and N fall on the same curve, implying that the same correlation length governs the system-size dependence of both χ_4^{peak} and τ . These results establish the existence of a single growing length scale that describes the growth of fluctuations and relaxation in the present system.

III. DISCUSSION AND CONCLUSIONS

The activity-mediated unjamming of a cell monolayer is critical for several biological processes, such as cancer metastasis, embryogenesis, and development. In the early stage of EMT, the junction molecules weaken, and cells become motile. We have studied this regime and shown that the nature of the unjamming transition does not change in the presence of activity: the structure-dynamics correlation holds, and dynamics is sub-Arrhenius. We have also characterized the higher-order correlation functions with changing p_0 . As the system matures, junctions become firm, the dynamics becomes progressively sluggish, and the length scale, ξ_d , and the DH volume, χ_4^{peak} , increases. Our results rationalize the existing experiments on confluent cell monolayers [8]. We have also shown that a growing length scale governs the growth of DH and the relaxation time and have obtained the exponents that

characterize the divergence of these quantities.

The structure-dynamics correlation has crucial significance. Many past works have demonstrated a remarkable correlation of cell shape with cellular functions, such as division plane orientation [61–63], cell growth or apoptosis [64], stem cell lineage [65, 66], and differentiation [67, 68]. In particular, cell division and apoptosis will affect the monolayer dynamics by cutting off the relaxation time [69–71]. Thus, the structure-dynamics correlation of confluent monolayers is consistent with these findings. Yet, cancer cells exhibit an intricate property: they avoid the inherent defense mechanism of cell extrusion and apoptosis and continue to divide [3, 72]. Does this have a structural signature at the level of cell shape? Cell extrusion requires the organization of the forces and displacements. Therefore, comparing cell shapes between extruding and non-extruding cancerous cells can be instructive. Our work demonstrating the survival of the quantitative nature of the structure-dynamics correlation in the presence of activity is a first step in this direction.

Beyond the biological relevance, confluent models are also intriguing due to their fascinating physics properties. Their glassy dynamics seems better suited for MCT [41, 73]. We have shown that $F_s(k, t)$ follows the time-temperature superposition principle of MCT (see SM), τ follows the power-law prediction with the same exponent as in equilibrium systems, and χ_4^{peak} also diverges as a power law at the same critical point. Furthermore, we present the first computation of the dynamic length scale, ξ_d , in confluent systems via a finite-size scaling analysis [59]. We find that $\xi_d \sim \tau^{1/3}$; this is consistent with the critical nature of MCT, where the diverging time scale accompanies the divergence of a length scale. Interestingly, our results show that $(2 - \eta) = 1/2$; this is much smaller than the values obtained in both MCT and simulations of passive particulate systems. We have also computed a static length, ξ_s , and found that ξ_d is proportional to ξ_s . This result suggests that, unlike particulate systems [59], a unique length scale governs the dynamics.

Acknowledgments

We thank Smarajit Karmakar and Thomas Voightmann for discussions. We acknowledge the support of the Department of Atomic Energy, Government of India, under Project Identification No. RTI 4007. SKN thanks SERB for grant via SRG/2021/002014.

[1] P. Steeg, *Nat. Met.* **12**, 895 (2006).
 [2] J. Fares, M. Y. Fares, H. H. Khachfe, H. A. Salhab, and Y. Fares, *Sig. Transduct. Target. Ther.* **5**, 28 (2020).
 [3] D. Wirtz, K. Konstantopoulos, and P. C. Searson, *Nat. Rev. Canc.* **11**, 512 (2011).
 [4] J. Lee, M. Stone, P. Porrett, *et al.*, *Nature* **567**, 249 (2019).
 [5] J. Massagué and A. Obenauf, *Nature* **529**, 298 (2016).

[6] L. Oswald, S. Grosser, D. M. Smith, and J. A. Käs, *J. Phys. D: Appl. Phys.* **50**, 483001 (2017).
 [7] J. A. Mitchel, A. Das, M. J. O’Sullivan, I. T. Stancil, S. J. DeCamp, S. Koehler, O. H. Ocaña, J. P. Butler, J. J. Fredberg, M. A. Nieto, D. Bi, and J.-A. Park, *Nat. Commun.* **11**, 5053 (2020).

- [8] J.-A. Park, J. H. Kim, D. Bi, J. A. Mitchel, N. T. Qazvini, K. Tantisira, C. Y. Park, M. McGill, S.-H. Kim, B. Gweon, J. Notbohm, R. S. Jr, S. Burger, S. H. Randell, A. T. Kho, D. T. Tambe, C. Hardin, S. A. Shore, E. Israel, D. A. Weitz, D. J. Tschumperlin, E. P. Henske, S. T. Weiss, M. L. Manning, J. P. Butler, J. M. Drazen, and J. J. Fredberg, *Nat. Mater.* **14**, 1040 (2015).
- [9] S. Sadhukhan, S. Dey, S. Karmakar, and S. K. Nandi, *Euro. Phys. J. Spec. Top.* (2024), 10.1140/epjs/s11734-024-01188-1.
- [10] M. Sadati, N. Taheri Qazvini, R. Krishnan, C. Y. Park, and J. J. Fredberg, *Differentiation* **86**, 121 (2013), mechanotransduction.
- [11] J.-A. Park, L. Atia, J. A. Mitchel, J. J. Fredberg, and J. P. Butler, *J. Cell Sci.* **129**, 3375 (2016).
- [12] T. E. Angelini, E. Hannezo, X. Trepas, M. Marquez, J. J. Fredberg, and D. A. Weitz, *Proc. Natl. Acad. Sci. (USA)* **108**, 4717 (2011).
- [13] A. Mongera, P. Rowghanian, H. J. Gustafson, E. Shelton, D. A. Kealhofer, E. K. Carn, F. Serwane, A. A. Lucio, J. Giammona, and O. Campàs, *Nature* (2018).
- [14] F. Schöck and N. Perrimon, *Annual Review of Cell and Developmental Biology* **18**, 463 (2002).
- [15] E. Hannezo, J. Prost, and J.-F. Joanny, *Proc. Natl. Acad. Sci. (USA)* **111**, 27 (2014).
- [16] A. Brugués, E. Anon, V. Conte, J. H. Veldhuis, M. Gupta, J. Colombelli, J. J. Muñoz, G. W. Brodland, B. Ladoux, and X. Trepas, *Nat. Phys.* **10**, 683 (2014).
- [17] K. D. Nnetu, M. Knorr, D. Strehle, M. Zink, and J. A. Käs, *Soft Matter* **8**, 6913 (2012).
- [18] M. Poujade, E. Grasland-Mongrain, A. Hertzog, J. Jouanneau, P. Chavrier, B. Ladoux, A. Buguin, and P. Silberzan, *Proc. Natl. Acad. Sci. (USA)* **104**, 15988 (2007).
- [19] T. Das, K. Safferling, S. Rausch, N. Grabe, H. Boehm, and J. P. Spatz, *Nat. Cell Biol.* **17**, 276 (2015).
- [20] P. Friedl and D. Gilmour, *Nat. Rev. Mol. Cell Biol.* **10**, 445 (2009).
- [21] S. Kumar and V. M. Weaver, *Cancer and Metastasis Reviews* **28**, 113 (2009).
- [22] D. Hanahan and R. Weinberg, *Cell* **144**, 646 (2011).
- [23] C. Malinverno, S. Corallino, F. Giavazzi, M. Bergert, Q. Li, M. Leoni, A. Disanza, E. Frittoli, A. Oldani, E. Martini, T. Lendenmann, G. Deflorian, G. V. Beznoussenko, D. Poulidakos, K. H. Ong, M. Uroz, X. Trepas, D. Parazzoli, P. Maiuri, W. Yu, A. Ferrari, R. Cerbino, and G. Scita, *Nat. Mater.* **16**, 587 (2017).
- [24] J. H. Kim, A. F. Pegoraro, A. Das, S. A. Koehler, S. A. Ujwary, B. Lan, J. A. Mitchel, L. Atia, S. He, K. Wang, D. Bi, M. H. Zaman, J.-A. Park, J. P. Butler, K. H. Lee, J. R. Starr, and J. J. Fredberg, *Biochemical and Biophysical Research Communications* **521**, 706 (2020).
- [25] J. P. Thiery, *Nat. Rev. Cancer* **2**, 442 (2002).
- [26] M. Théry and M. Bornens, *Current Opinion in Cell Biology* **18**, 648 (2006), cell division, growth and death / Cell differentiation.
- [27] H. Hugo, M. L. Ackland, T. Blick, M. G. Lawrence, J. A. Clements, E. D. Williams, and E. W. Thompson, *Journal of Cellular Physiology* **213**, 374 (2007).
- [28] M. Lu, M. K. Jolly, H. Levine, J. N. Onuchic, and E. Ben-Jacob, *Proc. Natl. Acad. Sci. (USA)* **110**, 18144 (2013).
- [29] J. Yang, P. Antin, G. Berx, *et al.*, *Nat. Rev. Mol. Cell Biol.* **21**, 341 (2020).
- [30] H. Z. Xiao-Jun Tian and J. Xing, *Biophys. J.* **105**, 1079 (2013).
- [31] J. Zhang, X. J. Tian, H. Zhang, Y. Teng, R. Li, F. Bai, S. Elankumar, and J. Xing, *Sci. Signal.* **7**, ra91 (2014).
- [32] M. K. Jolly, M. Boareto, B. Huang, D. Jia, M. Lu, *et al.*, *Front. Oncol.* **5**, 155 (2015).
- [33] D. Bi, X. Yang, M. C. Marchetti, and M. L. Manning, *Phys. Rev. X* **6**, 021011 (2016).
- [34] S. Sadhukhan, M. K. Nandi, S. Pandey, M. Paoluzzi, C. Dasgupta, N. Gov, and S. K. Nandi, *Soft Matter* **20**, 6160 (2024).
- [35] Y.-W. Li, L. L. Y. Wei, M. Paoluzzi, and M. P. Ciamarra, *Phys. Rev. E* **103**, 022607 (2021).
- [36] W. Gotze and L. Sjogren, *Reports on Progress in Physics* **55**, 241 (1992).
- [37] S. P. Das, *Rev. Mod. Phys.* **76**, 785 (2004).
- [38] L. M. C. Janssen, *Front. Phys.* **6**, 1 (2018).
- [39] L. Atia, D. Bi, Y. Sharma, J. A. Mitchel, B. Gweon, S. A. Koehler, S. J. DeCamp, B. Lan, J. H. Kim, R. Hirsch, A. F. Pegoraro, K. H. Lee, J. R. Starr, D. A. Weitz, A. C. Martin, J.-A. Park, J. P. Butler, and J. J. Fredberg, *Nat. Phys.* **14**, 613 (2018).
- [40] S. Sadhukhan and S. K. Nandi, *eLife* **11**, e76406 (2022).
- [41] S. Pandey, S. Kolya, D. Padmashree, S. Sadhukhan, T. Das, and S. K. Nandi, *arXiv* **v1**, 2306.07250 (2023).
- [42] P. J. Albert and U. S. Schwarz, *Cell Adhesion & Migration* **10**, 516 (2016), pMID: 26838278.
- [43] R. Farhadifar, J.-C. Röper, B. Aigouy, S. Eaton, and F. Jülicher, *Curr. Biol.* **17**, 2095 (2007).
- [44] A. G. Fletcher, M. Osterfield, R. E. Baker, and S. Y. Shvartsman, *Biophys. J.* **106**, 2291 (2014).
- [45] G. Parisi, *Nature* **433**, 221 (2005).
- [46] S. K. Nandi and N. S. Gov, *Soft Matter* **13**, 7609 (2017).
- [47] E. Flenner, G. Szamel, and L. Berthier, *Soft Matter* **12**, 7136 (2016).
- [48] L. Berthier, E. Flenner, and G. Szamel, *J. Chem. Phys.* **150**, 200901 (2019).
- [49] K. Paul, A. Mutneja, S. K. Nandi, and S. Karmakar, *Proc. Natl. Acad. Sci. (USA)* **120**, e2217073120 (2023).
- [50] G. Szamel and E. Flenner, *Phys. Rev. E* **74**, 021507 (2006).
- [51] P. Pareek, M. Adhikari, C. Dasgupta, and S. K. Nandi, *J. Chem. Phys.* **159**, 174503 (2023).
- [52] A. Einstein, *Investigations on the theory of the Brownian Movement* (Dover Publications, INC., New York, 1956).
- [53] M. T. Cicerone and M. D. Ediger, *J. Chem. Phys.* **104**, 7210 (1996).
- [54] E. Flenner and G. Szamel, *Phys. Rev. E* **72**, 031508 (2005).
- [55] H. S. Ansell, C. Li, and D. M. Sussman, *arXiv* , 2409.00496 (2024).
- [56] S. K. Nandi and S. Ramaswamy, *Phys. Rev. Lett.* **109**, 115702 (2012).
- [57] G. Biroli, J.-P. Bouchaud, K. Miyazaki, and D. R. Reichman, *Phys. Rev. Lett.* **97**, 195701 (2006).
- [58] M. Kardar, *Statistical Physics of Fields* (Cambridge University Press, 2019).
- [59] S. Karmakar, C. Dasgupta, and S. Sastry, *Proceedings of the National Academy of Sciences* **106**, 3675 (2009).
- [60] S. Karmakar, C. Dasgupta, and S. Sastry, *Phys. Rev. Lett.* **105**, 015701 (2010).
- [61] T. P. J. Wyatt, A. R. Harris, M. Lam, Q. Cheng, J. Bellis, A. Dimitracopoulos, A. J. Kablae, G. T. Charras, and B. Baum, *Proc. Natl. Acad. Sci. (USA)* **112**, 5726 (2015).
- [62] K. C. Hart, J. Tan, K. A. Siemers, J. Y. Sim, B. L. Pruitt, W. J. Nelson, and M. Gloerich, *Proc. Natl. Acad. Sci. (USA)* **114**, E5845 (2017).
- [63] F. Bosveld, O. Markova, B. Guirao, C. Martin, Z. Wang, A. Pierre, M. Balakireva, I. Gague, A. Ainslie, N. Christophorou, D. K. Lubensky, N. Minc, and Y. Bellaïche, *Nature* **530**, 495 (2016).
- [64] C. S. Chen, M. Mrksich, S. Huang, G. M. Whitesides, and D. E. Ingber, *Science* **276**, 1425 (1997).

- [65] R. McBeath, D. M. Pirone, C. M. Nelson, K. Bhadriraju, and C. S. Chen, *Dev. Cell* **6**, 483 (2004).
- [66] Y.-K. Wang, X. Yu, D. M. Cohen, M. A. Wozniak, M. T. Yang, L. Gao, J. Eyckmans, and C. S. Chen, *Stem Cells. Dev.* **21**, 1176 (2011).
- [67] F. M. Watt, P. W. Jordan, and C. H. O'Neill, *Proc. Natl. Acad. Sci. (USA)* **85**, 5576 (1988).
- [68] C. D. Roskelley, P. Y. Desprez, and M. J. Bissell, *Proc. Natl. Acad. Sci. (USA)* **91**, 12378 (1994).
- [69] J. Ranft, M. Basan, J. Elgeti, J.-F. Joanny, J. Prost, and F. Jülicher, *Proc. Natl. Acad. Sci. (USA)* **107**, 20863 (2010).
- [70] M. Czajkowski, D. M. Sussman, M. C. Marchetti, and M. L. Manning, *Soft Matter* **15**, 9133 (2019).
- [71] D. A. Matoz-Fernandez, K. Martens, R. Sknepnek, J. L. Barrat, and S. Henkes, *Soft Matter* **13**, 3205 (2017).
- [72] D. Cai, Z. Liu, and J. Lippincott-Schwartz, "Biomolecular condensates and their links to cancer progression," (2021).
- [73] C. Ruscher, S. Ciarella, C. Luo, L. M. C. Janssen, J. Farago, and J. Baschnagel, *J. Phys.: Condens. Matter* **33**, 064001 (2021).
- [74] J. Prost, F. Jülicher, and J.-F. Joanny, *Nature Physics* **11**, 111 (2015).
- [75] J. A. Glazier and F. Graner, *Phys. Rev. E* **47**, 2128 (1993).
- [76] F. Graner and J. A. Glazier, *Phys. Rev. Lett.* **69**, 2013 (1992).
- [77] P. Hogeweg, *J. Theor. Biol.* **203**, 317 (2000).
- [78] H. Honda, H. Yamanaka, and M. Dan-Sohkawa, *Journal of Theoretical Biology* **106**, 423 (1984).
- [79] A. G. Fletcher, J. M. Osborne, P. K. Maini, and D. J. Gavaghan, *Prog. Biophys. Mol. Biol.* **113**, 299 (2013).
- [80] M. Paoluzzi, L. Angelani, G. Gosti, M. C. Marchetti, I. Pagonabarraga, and G. Ruocco, *Phys. Rev. E* **104**, 044606 (2021).
- [81] H. P. Jain, A. Voigt, and L. Angheluta, *Scientific Reports* **13**, 10096 (2023).
- [82] D. Wenzel and A. Voigt, *Phys. Rev. E* **104**, 054410 (2021).
- [83] M. Nonomura, *PLoS ONE* **7**, e33501 (2012).
- [84] W. Götze, *Complex Dynamics of Glass-Forming Liquids: A Mode-Coupling Theory* (Oxford University Press, 2008).

Supplementary Materials for Nature of the activity-mediated unjamming transition in confluent cell monolayers

Souvik Sadhukhan¹, Chandan Dasgupta², Saroj Kumar Nandi¹

¹Tata Institute of Fundamental Research, 36/P Gopanally Village, Hyderabad - 500046, India

²Department of Physics, Indian Institute of Science, Bangalore 560012, India; International Centre for Theoretical Sciences, TIFR, Bangalore 560089, India

S1. Model and Simulation Details

The effective energy function of a single-component confluent monolayer is

$$\mathcal{H} = \sum_{i=1}^N [\lambda_A (a_i - a_0)^2 + \lambda_P (p_i - p_0)^2], \quad (\text{S1})$$

where N is the total number of cells. a_i and p_i are the area and the perimeter of the i th cell. a_0 and p_0 are the target area and perimeter of the cells. As stated in the main text, we have taken a 50:50 binary mixture with an average area $a_0 = 1$. The cell cytoplasm can be treated as an incompressible fluid [74], and the monolayer height remains nearly constant [43]. These two properties lead to the area constraint with a strength λ_A , the first term in Eq. (S1). On the other hand, the second term in Eq. (S1) is a combination of two terms: the linear term in p_i is a result of the cell-cell adhesion and the cortical tension, and the quadratic term in p_i signifies the actomyosin contractility. $a_0 = 1$ sets the length scale of the system.

Given the energy function, Eq. (S1), we now need a model of confluent systems. Several such models exist to study the static and dynamic properties. Examples include, the cellular Potts model (CPM) [75–77], Vertex [44, 78, 79] and Voronoi models [33, 80], Phase field models [81–83] etc. For this study, we have used the active athermal Vertex model (AVM). We have used molecular dynamics simulation by integrating the over-damped equation of motion for each vertex l given by,

$$\frac{d\mathbf{r}_l}{dt} = \mu^{-1} (\mathbf{F}_l + \tilde{\mathbf{f}}_l), \quad (\text{S2})$$

where μ is the friction, set to 1, $\mathbf{F}_l = -\nabla_l \mathcal{H}$ is the force due to the energy function in Eq. (1). $\tilde{\mathbf{f}}_l$ is the active force acting on vertex l of the i^{th} cell: $\tilde{\mathbf{f}}_l = \frac{v_0}{3} \sum_{j \in \mathcal{N}(l)} \hat{\mathbf{n}}_j$, where $\mathcal{N}(l)$ is the number of all neighbouring cells sharing vertex l and $\hat{\mathbf{n}}_i = (\cos \phi_i, \sin \phi_i)$. $\phi_i(t)$ is the angle of the motile force with the x -axis. It performs a random rotational diffusion with a diffusion constant D_r ,

$$\partial_t \phi_i(t) = \sqrt{2D_r} \eta_i(t), \quad (\text{S3})$$

where, η_i is a Gaussian white noise with zero mean and variance $\langle \eta_i(t) \eta_j(t') \rangle = \delta(t - t') \delta_{ij}$. D_r is proportional to the inverse of the persistence time τ_p . We have used the Euler-Murayama integration scheme to evolve the vertices. We have averaged the data over 100 time-origins and 32 ensembles. We have used a binary 50 : 50 mixture of cells to avoid crystallization. This binary system is designated by p_0 given by: $p_0 = p_{0\alpha} / \sqrt{a_{0\alpha}} = p_{0\beta} / \sqrt{a_{0\beta}}$. We show a typical snapshot of our system in Fig. S1.

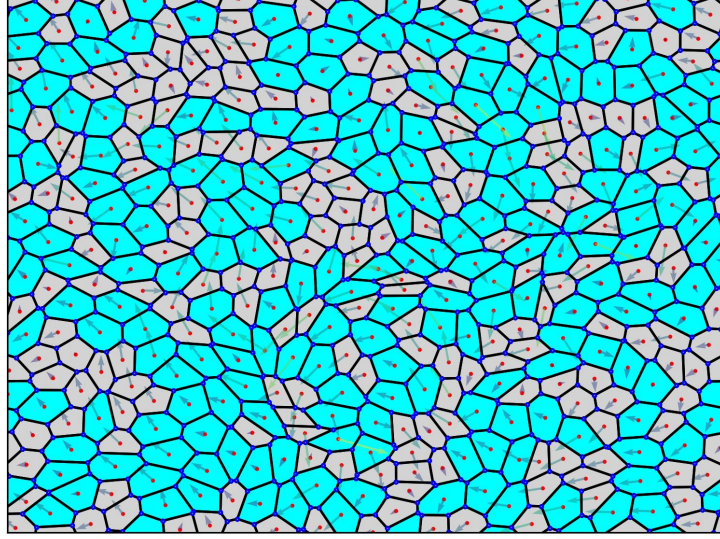


FIG. S1. A typical snapshot from our simulations of the self-propelled Vertex model. We have associated color to each cell according to its target area $a_{0\alpha}$ or $a_{0\beta}$. The arrows denote their instantaneous velocity direction.

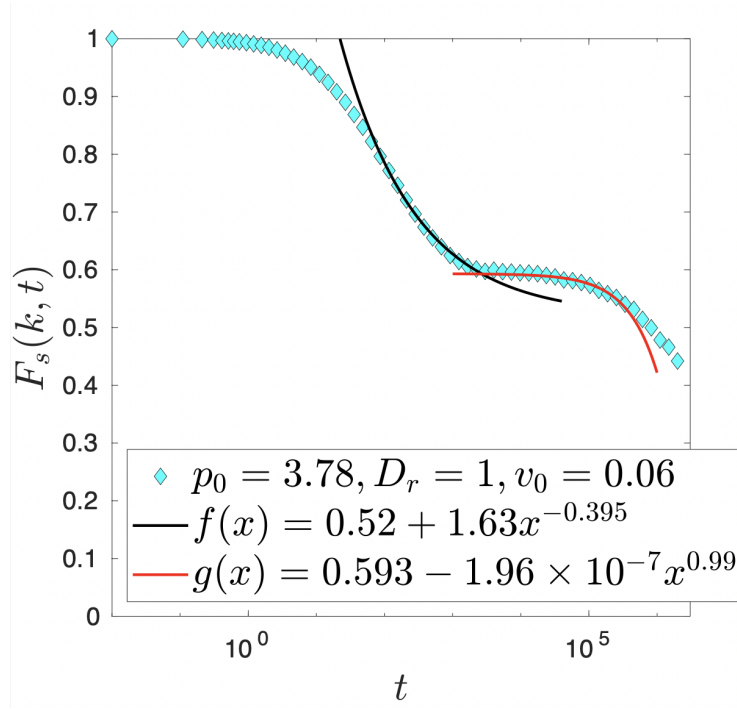


FIG. S2. Test of the MCT prediction for the β -relaxation of $F_s(k, t)$. Symbols are the plot of $F_s(k, t)$ for $p_0 = 3.78$, $v_0 = 0.06$ and $D_r = 1$. We have separately fitted the early and late β -regimes with Eq. (S5) (black and red lines). We obtain the parameters as follows: $f = 0.52$, $A = 1.63$, and $a = 0.395$ for the early β -regime and $f = 0.593$, $B = 1.96 \times 10^{-7}$, and $b = 0.99$ for the late β -regime.

S2. Determination of MCT Scaling Exponents: a , b , and γ

As discussed in the main text, we characterized the dynamics via the two-point self-intermediate scattering function, $F_s(k, t)$,

$$F_s(k, t) = \langle \tilde{F}_s(k, t) \rangle = \frac{1}{N_\alpha} \left\langle \sum_{i=1}^{N_\alpha} \exp[i\mathbf{k} \cdot (\mathbf{r}_i(0) - \mathbf{r}_i(t))] \right\rangle. \quad (\text{S4})$$

For our binary system, we could define two different $F_s(k, t)$, one for each type of particle. They contain the same information [50]. Here, we present the results for only the α -particles. We have chosen $k \simeq k_{max}$, the wavevector corresponding to the maximum of the static structure factor. We have obtained the relaxation time τ when $F_s(k, t)$ decays to 0.3.

MCT predicts that τ diverges as a power law with an exponent γ . For an athermal active system $T \sim v_0^2$ and the relation modifies as $\tau \propto (v_0^2 - v_c^2)^{-\gamma}$. γ is obtained by fitting the data in experiments and simulations. MCT also predicts a power-law decay for the β -regime. The early and late β -regimes of $F_s(k, t)$ are characterized by two exponents, a and b :

$$F_s(k, t) = \begin{cases} f + At^{-a}, & \text{for early } \beta\text{-regime,} \\ f - Bt^b, & \text{for late } \beta\text{-regime.} \end{cases} \quad (\text{S5})$$

where f , A , and B are constants [36, 84]. Close to the MCT transition point, a and b are related as,

$$\frac{\Gamma^2(1-a)}{\Gamma(1-2a)} = \frac{\Gamma^2(1+b)}{\Gamma(1+2b)}, \quad (\text{S6})$$

where Γ is the Gamma function. Furthermore, MCT also predicts a relation between a , b , and γ :

$$\gamma = \frac{1}{2a} + \frac{1}{2b}. \quad (\text{S7})$$

We have tested this prediction of MCT. Figure (S2) shows the fit with the data for $p_0 = 3.78$ and $v_0 = 0.06$. We find that the values of a and b remain nearly constant: $a = 0.395$ and $b = 0.99$. Using these values, we find that Eq. (S6) is valid up to the second order. In addition, we obtain $\gamma = 1.77$ from Eq. (S7). This value is slightly higher than that obtained from the relaxation time data.